Journal of Materials Chemistry

Cite this: J. Mater. Chem., 2011, 21, 13032

www.rsc.org/materials

PAPER

Synthesis of bulk and nanoporous carbon nitride polymers from ammonium thiocyanate for photocatalytic hydrogen evolution†

Yanjuan Cui,[a] Jinshui Zhang,[a] Guigang Zhang,[a] Jianhui Huang,[a] Ping Liu,[a] Markus Antonietti[b] and Xinchen Wang*[ab]

Received 4th May 2011, Accepted 15th June 2011
DOI: 10.1039/c1jm11961c

Graphitic carbon nitride was synthesized by direct thermal polymerization of ammonium thiocyanate as the precursor. The transfer of this simple thermal-induced polymerization onto hard-templates with various nanoarchitectures enables the fabrication of nanostructured carbon nitrides *via* a soft-chemical synthesis, while the involvement of a sulfur species within the reaction cascade offers additional chemical control of the texture and the electronic structures. The catalysts were subjected to several characterizations, and the results obtained revealed that nanoporous carbon nitrides can be obtained by templating with nanosized silica and SBA-15. Photocatalytic activity was evaluated toward hydrogen evolution from proton solution with visible light. Results show that g-C_3N_4 synthesized from ammonium thiocyanate exhibited improved photoactivity in comparison with g-C_3N_4 obtained from dicyandiamide. Further improvement in the activity was achieved by creating the nanostructures in g-C_3N_4. This is due to the enhanced surface area obtained which is favorable for light-harvesting and mass-transfer, as well as to the increased redox potential.

1. Introduction

The search for renewable energy as an alternative to fossil fuels is attracting renewed attention, owing to the increasing energy demands and concerns on climate change related to CO_2 emissions.[1,2] Solar energy has been regarded as an ideal clean energy source not only to meet the world's long-term energy needs but also to solve climate problems, provided that sunlight can be captured, converted and stored in a cost-effective fashion.[3,4] Among various types of solar energy conversion, solar chemical conversion (converting solar energy to chemical fuels) has been actively investigated with hope of transferring biological photosynthesis to a manmade environment with a higher efficiency than plants.[1]

Semiconductor-mediated photocatalysis allows for direct solar chemical conversion by water photosplitting[5–10] or CO_2 photofixation,[11–14] as such solar energy is converted and stored in energy-rich molecules, such as hydrogen, sugars, and hydrocarbons. Solar hydrogen is the preferable basis of an environmentally-acceptable and infinite energy system, which can free mankind from the fossil resources, forever. Since the discovery of hydrogen generation from water by TiO_2-based photoelectrochemical cells in 1972,[5] enormous efforts have been made to establish a stable photocatalytic water splitting system by minimizing the device down to a nanopowder system free of extra bias.[15–17] The heterogeneous powder system is believed to enable large-scale hydrogen generation from water using sunlight. To this end, the central problem is to design and develop sustainable materials as photocatalysts that should be efficient, stable, inexpensive as well as reactive with visible light, thus by far remains a challenge.

Over the past 40 years, hundreds of inorganic semiconductors have been tested as water splitting photocatalysts, including binary and ternary metal oxides.[18,19] However, most of these oxide catalysts only work with UV-light irradiation due to their intrinsic large band gap (typically >3 eV), which confines the utilization of sunlight with wavelengths below 412 nm, only. Although some inorganic semiconductors including metal (oxy) nitrides and metal (oxy)sulfides are reported to be active with high stability under visible light excitation, most of them contain expensive and/or precious metal components, like Ga, Ge, Ta, In and so on.[6,20–22] Recently, notable advances in heterogeneous photocatalysis have been made using metal-free, polymeric carbon nitrides as light antennae to mediate electron and energy transfers for artificial photosynthesis.[23] Covalent carbon nitride solid is a well-known material that has attracted worldwide research interest of physicists, chemists, and material scientists because the incorporation of nitrogen atoms in the carbon

[a]*International Joint Laboratory, Research Institute of Photocatalysis, State Key Laboratory Breeding Base of Photocatalysis, Fuzhou University, Fuzhou, 350002, People's Republic of China. E-mail: xcwang@fzu.edu.cn; Fax: +86-591-83738608*
[b]*International Joint Laboratory, Max-Planck Institute of Colloids and Interfaces, Department of Colloid Chemistry, Research Campus Golm, 14424 Potsdam, Germany*

† Electronic supplementary information (ESI) available: The SEM and TEM images of SBA-15; elemental composition of the sample obtained from CHN analysis and H_2 evolution rate of mpg-$CN_{0.2}$ synthesized at different temperatures. See DOI: 10.1039/c1jm11961c

nanostructure can theoretically enhance the mechanical, conducting, field-emission, energy-storage and catalytic properties.[24–27] It was found that graphitic carbon nitride (g-C_3N_4) exhibits high thermal and chemical stability in contact with oxygen and water, being a two-dimensional π-conjugated semiconductor capable of creating charged carriers with light. An infinite g-C_3N_4 sheet is calculated to feature a 2.6 eV band gap with absolute band positions engulfing the H_2O redox potentials[23] and in principle it is a suitable alternative photocatalyst to catalyze the full water cleavage reaction. Our previous investigations on carbon nitride photocatalysis have indeed confirmed that g-C_3N_4 is able to liberate H_2 or O_2 from water with visible light, in the presence of an electron donor and acceptor for both half reactions, respectively.[23,28,29]

Carbon nitride solids are typically synthesized by high-temperature and high-pressure routes using diverse physical and chemical methods. Recently, the thermal-induced polycondensation of simple organic monomers has also been adopted to synthesize various modifications of carbon nitride solids. A remarkable benefit of the chemical synthesis of carbon nitride polymers is that they can be readily combined with the well-established template processes to control the textural structure of carbon nitrides. For example, Vinu *et al.* recently reported the preparation of highly ordered mesoporous nitrogen-doped carbons with tunable pore size and an N/C atomic ratio of 0.2 using mesoporous silica SBA-15 as a template.[30–32] Nanoporous graphitic C_3N_4 with higher nitrogen content have also been developed: the mesoporosity and macroporosity were successfully imparted into g-C_3N_4 frameworks by heating the mixture of cyanamide and different-sized silica particles, followed by removal of the silica template with HF.[33–35] Ordered hexagonal and cubic mesoporous graphitic carbon nitride with high N/C atomic ratio of 0.7 has also been fabricated using ordered mesoporous silica SBA-15 and KIT-6 as hard templates from cyanamide.[36,37] These mesoporous carbon nitrides with unique semiconductive properties along with large surface areas, small particle size, and tunable pore diameters, promise access to an even wider range of applications due to their interesting electrical and conducting properties.

The synthesis of g-C_3N_4 materials covers a wide range of liquid and solid nitrogen-containing organic compounds. Cyanamide, melamine and other *s*-triazine (C_3N_3) heterocyclic compounds such as $C_3N_3X_3$ (X = Cl, N, OH, NHCl) have been mainly employed as the molecular precursors for C_3N_4 graphitic phase.[38,39] However, most of these *s*-triazine ring monomers either possess low aqueous solubility or are susceptible to hydrolysis in an uncontrolled manner, whereas cyanamide is an irritant and is expensive. The search for new starting materials for carbon nitride is therefore still a very active topic. Historically, artificial carbon nitride was first obtained by Beruriwuz from the lighting of mercuric thiocyanate in 1830, and in 1834 it was named "melon" by Liebig.[40] In 1922, Franklin also described the formation of an amorphous C/N material with its composition close to C_3N_4 by thermolysis of mercuric thiocyanate.[41] In another report from 1972, lanthanum thiocyanate was found to decompose at 400 °C, producing C_3N_4.[42] We recently also introduced a sulfur-containing organic compound, trithiocyanuric acid, as a starting monomer for carbon nitride, and found that the sulfur-mediated synthesis offers less terminal groups in the polymeric structure and is thereby a promising tool for the control of the optical and electronic properties of carbon nitride semiconductors, as well as their photocatalytic functions.[29] However, efforts to fabricate porous C_3N_4 using this precursor failed.

In this paper, we describe the use of ammonium thiocyanate, an inexpensive salt with high solubility in water, as a metal-free thiocyanate precursor for carbon nitride synthesis. This sulfur-containing CN_x-precursor allows the easy control of nano/mesostructures with various hard templates due to its water-compatible ionic character, while still keeping the advantages of sulfur-mediated synthesis of graphitic carbon nitride at later stages of reaction to complete the two-dimensional condensation.

2. Experimental section

2.1. Preparation of graphitic carbon nitrides

Bulk g-C_3N_4 was prepared by directly heating ammonium thiocyanate (AT) at different temperatures under a nitrogen atmosphere and then tempering at this temperature for another 2h. The sample thus prepared was denoted as g-C_3N_4 (AT). Dicyandiamide (DCDA) was also heated to 550 °C under the same conditions to obtain a traditional g-C_3N_4 as a reference sample denoted as g-C_3N_4 (DCDA).

To prepare mesoporous graphitic carbon nitride (mpg-CN_r-*T*, *r* refers to the initial silica/AT mass ratio, *T* refers to the calcination temperature, and if not denoted, *T* refers to 550 °C), NH_4SCN (10 g, Sinopharm Chemical Reagent Co., Ltd) was dissolved in 10 mL H_2O, followed by dropping a certain amount of a 40% dispersion of 12 nm SiO_2 particles in water (Ludox HS40, Aldrich, 10 g Ludox for the sample with $r = 0.4$). The resulting mixtures were stirred at 100 °C to remove water. The dry solid was subjected to sintering at 550 °C for 2 h in a muffle furnace. The resultant yellow powder was treated with NH_4HF_2 (4 M) aqueous solution to remove the silica template. The powders were then washed with distilled water and ethanol several times. Finally, the powers were dried at 60 °C in air overnight.

Ordered mesoporous graphitic carbon nitride (ompg-CN) was prepared using SBA-15 and ammonium thiocyanate as the hard template and CN_x-precursor, respectively. SBA-15 was obtained using Pluronic P123 and tetraethylorthosilicate (TEOS) according to the method reported before.[43] In a typical synthesis, 2.79 g TEOS was mixed with 1.73 g P123 in 1.6 M HCl solution and stirred at 35 °C for 24 h. The mixture was heated to 150 °C and maintained at this temperature for 24 h under static conditions in a Teflon-lined autoclave. The resultant precipitate was washed and dried at 60 °C overnight, followed by a further calcination at 550 °C in air for 6 h. ompg-C_3N_4 was prepared by a template-assisted approach.[31] In a typical synthesis, 1.5 g of the SBA-15 was added to NH_4SCN aqueous solution (0.013 M) and stirred for 1 h. The resultant mixture was filtered, dried in air, and finally calcinated at 550 °C for 2 h. The template was subsequently removed using NH_4HF_2 (4 M), followed by filtered, washed with water and ethanol several times, and finally dried at 60 °C overnight.

2.2. Characterization

X-ray diffraction (XRD) patterns were collected using a Bruker D8 Advance X-ray diffractometer (Cu-Kα_1 irradiation, λ = 1.5406 Å). A Varian Cary 500 Scan UV-Vis spectrophotometer was used to record the UV-Vis diffuse reflectance spectra of different samples with barium sulfate as the reference sample. Fourier transformed infrared (FTIR) spectra were recorded using a Nicolet Magna 670 FTIR spectrometer, and the samples were mixed with KBr at a concentration of *ca.* wt. 1%. N_2-adsorption-desorption analyses were carried out at 77 K using Mocromeritics ASAP 2010 equipment. X-ray photoelectron spectroscopy (XPS) data were obtained with a Thermo ESCA-LAB250 instrument with a monochromatized Al Kα line source (200 W). The thermal stability of the as-prepared samples was verified using a thermogravimetric analyzer (Perkin-Elmer TGA7). Elemental analysis results were collected from a Vario MICRO. The morphology of the sample was investigated by field emission scanning electron microscopy (SEM) (JSM-6700F). Transmission electro microscopy (TEM) was carried out using a JEOL model JEM 2010 EX instrument. Electrochemical measurements were conducted with a BAS Epsilon Electro-chemical System in a conventional three electrode cell, using a Pt plate as the counter electrode and Ag/AgCl electrode (3 M KCl) as the reference electrode.

2.3. Photocatalytic activity for hydrogen evolution.

Reactions were carried out in a Pyrex topped-irradiation reaction vessel connected to a glass closed gas system. H_2 production was performed by dispersing 50 mg of catalyst powder in an aqueous solution (100 mL) containing triethanolamine (5 vol.%) as a sacrificial electron donor. 3 wt.% Pt was loaded on the surface of the carbon nitride sample by the *in situ* photodeposition method using H_2PtCl_6. The reaction solution was evacuated several times to remove air completely prior to irradiation under a 300 W Xeon-lamp and a water filter. The wavelength of the incident light was controlled by applying an appropriate long-pass cut-off filter (λ > 420 nm). The temperature of the reaction solution was maintained at room temperature by a flow of cooling water during the reaction. The evolved gases were analyzed by gas chromatography equipped with a thermal conductive detector (TCD) and a 5 Å molecular sieve column, using argon as the carrier gas.

3. Results and discussion

Fig. 1 gives the XRD patterns and FTIR spectra of bulk g-C_3N_4 synthesized at different temperatures. For comparison, the data of the starting material ammonium thiocyanate (NH_4SCN) are also presented in Fig. 1. The XRD patterns in Fig. 1a indicate that the typical graphite-like structure of g-C_3N_4 gradually evolves when the calcination temperature exceeds 450 °C. The strongest XRD peak at 27.0° is a characteristic inter-layer stacking reflection of conjugated aromatic systems, indexed for graphitic materials as the (002) peak. A rather tight stacking distance of the aromatic units of d = 0.329 nm can be calculated. When the sintering temperature is higher than 500 °C, the (002) peak is shifted slightly to a larger 2θ angle of 27.3° (corresponding to a calculated layer compression of d = 0.326 nm),

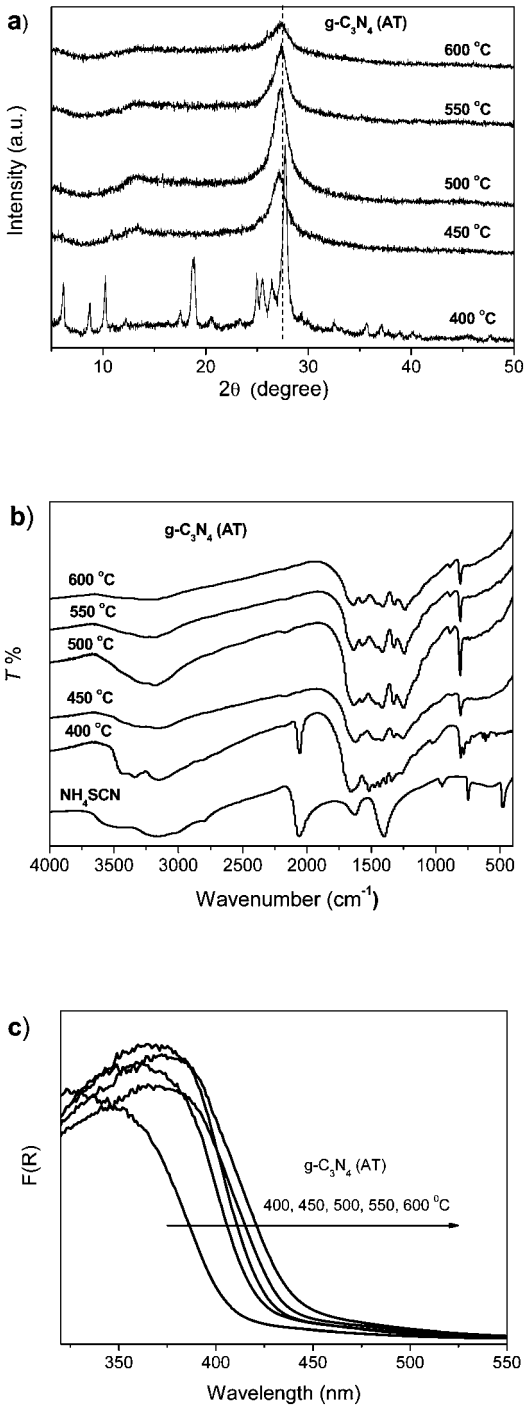

Fig. 1 a) XRD and b) FTIR c) UV-vis DRS for bulk C_3N_4 (AT) calcined at different temperatures.

indicating a structural compaction as the result of a better polycondensation of carbon nitride sheets at this elevated temperature.

The stacking (d = 0.326 nm) is more dense than the packing in crystalline graphite with its larger interlayer distance of d = 0.335 nm. The other pronounced XRD peak at 13.1° corresponds to a distance of d = 0.675 nm and can be assigned to an in-plane structural repeating motif, such as the void-to-void distance in the continuous heptazine network.[44] Further

increasing the temperatures to 550 and 600 °C weakens the peak at 27.3° gradually while the peak at 13.1° disappears slowly. This is an indication of the onset of thermal decomposition of the as made polymer. Decomposition occurs at a temperature of around 50 °C lower than that for ordinary C_3N_4 made from cyanamide, we attribute this to the altered local packing motifs or the complete release of sulphur species at a high thermodynamic force. The release of the atomically too large sulphur during the carbon nitride condensation has been found in previous work to influence the conformation and the connectivity of the resultant C_3N_4 sheets, leading to the broadening and weakening of the XRD peaks at 27.3°.[29] This bending offers an important chemical tool to tune the physical and chemical properties of carbon nitride polymers, and hence to adjust their photocatalytic functions.

Typical FTIR spectra of bulk g-C_3N_4 prepared at different temperatures are displayed in Fig. 1b. The spectrum of ammonium thiocyanate as the precursor for carbon nitride synthesis is also given for direct comparison. For the g-C_3N_4 sample synthesized at 400 °C, we can easily observe the bands in the 1200–1700 cm^{-1} and 810 cm^{-1} region attributable to organic molecules containing tri-*s*-triazine ring moieties, but coexisting with the strong absorptions near 2060 cm^{-1} and 480 cm^{-1} corresponding to –SCN and C–S band vibrations, respectively. When the temperature increases to 450 °C, these absorption bands (related to –SCN and C–S) virtually disappeared, while the main absorption band of C–N modes at 1300 cm^{-1} and C=N modes near 1550 cm^{-1} became slightly stronger. At this temperature, practically complete desulphurization takes place. The sharp peak at 1640 cm^{-1} is regarded as a strong indication of good crystallinity of the graphitic C_3N_4 phase. The signals at 810, 1258, 1424, and 1635 cm^{-1} can be assigned to the skeletal vibrations of heptazine heterocyclic ring (C_6N_7) unites. Absorbance in the region of 3200–3400 cm^{-1} is related to residual N–H components and the O–H band is assignable to uncondensed amino groups and absorbed H_2O molecules, respectively. These results are in fairly good accordance with recent reports of carbon nitride materials prepared by polycondensation and polymerization reactions.[45–47] These spectra clearly prove that NH_4SCN molecules can undergo self-cyclization, polymerization and condensation processes to construct a heterocyclic C_6N_7 triazine ring system, while releasing H_2S and NH_3 (as shown in Scheme 1): the band of C≡N trimerizes and vanishes, then the band of C–N and C=N is rebuilt, element S escapes as H_2S, and the thus formed dimelamine condenses to produce the carbon nitride network *via* the deamination route. This process is very similar to the polymerization scheme of cyanamide, but the involvement of –SH as a fast leaving group provides accelerated and improved condensation of the materials. The element analysis results revealed that the samples synthesized at 500 and 600 °C possess a virtually neglegible content of S. That is to say graphitic carbon nitride could be produced by heating NH_4SCN directly without using any catalysts.

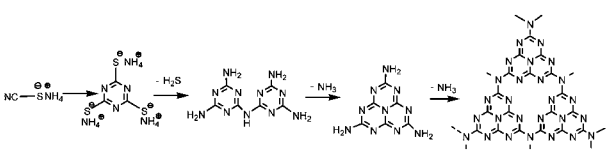

Scheme 1 Proposed self-polymerization of NH_4SCN to the carbon nitride network at high temperature.

Fig. 1c shows the optical properties of bulk g-C_3N_4 samples synthesized at different temperature, as investigated by UV-Vis diffuse reflectance spectroscopy. All samples demonstrate semiconductor-like absorptions in the blue visible light range. The fast rise in the optical absorption at ~430 nm is due to the excitation of the electron in the valence band to the conduction band. Increasing the heating temperature from 450 °C to 600 °C induces the gradual red-shift of the band edges from 425 nm to 450 nm, due to the enlargement of electron delocalization in the aromatic sheets associated with a higher degree of condensation at higher temperatures.

XPS is well-known to be sensitive to the chemical environments of light elements and has shown some utility in investigating the structural environments of covalent carbon nitride.[48] Fig. 2 gives the XPS spectra of our sample synthesized from ammonium thiocyanate as the precursor. Signals of the elements C, N, O are displayed but no peak assigned to S $2p_{1/2}$ (165 eV) can be seen in the spectrum survey (Fig. 2a). Higher resolution spectra were taken on the C_{1s}, N_{1s} and S_{2p} regions. The C_{1s} spectra in Fig. 2b show two peaks centering at 284.6 and 288.0 eV, while the 288.0 eV peak is the main contribution, which is identified as originating from sp^2-hybridized carbon in the aromatic ring attached to the $-NH_2$ group. The C_{1s} peak at 284.6 eV in the sample is typically assigned to graphitic carbon in the literature, but can also be attributed to sp^2 C–N.[49] The N_{1s} spectra in Fig. 2c can be deconvoluted into three peaks. The main component is centered at 398.6 eV attributable to sp^2 N involved in triazine rings, whereas the contribution at 400.1 eV corresponds to bridging nitrogen atoms N–(C)3. Charging effects or positive charge localization in heterocycles can lead to the peak at 404.4 eV.[50] Fig. 2d clearly indicated that no signals of S 2p ($2p_{3/2}$ = 164.0 eV) are found, which support the absence of S in

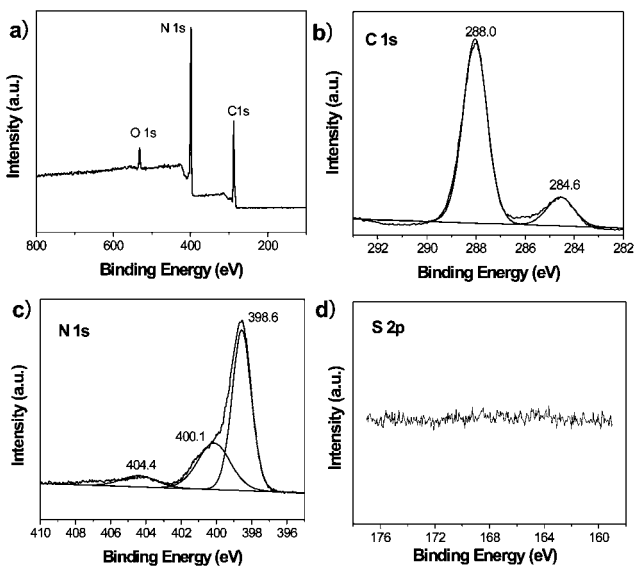

Fig. 2 XPS survey spectrum of graphitic carbon nitride synthesized from ammonium thiocyanate as the precursor a) and the corresponding high-resolution XPS spectra of C 1s b), N 1s c) and S 2p d).

the final product of g-C_3N_4, in good agreement with the chemical analysis. Since graphitic carbon nitride can obviously be efficiently synthesized from ammonium thiocyanate by a simple heat treatment, we extended this water-processable precursor to synthesize mesoporous and ordered mesoporous carbon nitride by integrating with the template-assisted method. The thermally-induced self-condensation of ammonium thiocyanate was therefore carried out on the surface of nano-sized silica particles and mesoporous SBA-15 as hard templates, followed by the removal of the templates, and hence the nano-sized pore was copied in the carbon nitride polymeric framework (see Scheme 2).

XRD patterns give typical (002) stacking peaks for all mpg-$CN_{0.2}$ samples sintered at different temperatures as shown in Fig. 3a, indicating the formation of a graphitic C_3N_4 phase at temperatures higher than 450 °C also in the presence of a template. The broadening and weakening of (002) reflection for the mpg-$CN_{0.2}$-600 samples suggested that the graphitic structure starts to turn thermally labile at this temperature. The FTIR spectra of the mpg-CN samples are shown in Fig. 3b and present skeletal vibrations of the heptazine heterocyclic ring. However, an obvious signal at 2180 cm^{-1} assigned to the appearance of C≡N or N=C=N,[51] which is not favourable for the formation of an inorganic network structure of carbon nitride materials since the existence of C≡N bonding would break the continuity of the network structure. This means that the mesoporous materials have a less extensively condensed framework, with more pending nitrile groups. In addition, no absorption bands associated with the silica template (*e.g.*, at 1000–1200 cm^{-1} owing to *v* Si–O–Si) can be observed, indicating that the silica could be completely removed. To support the absence of silica and to reanalyze the thermal stability of the samples, we carried out the thermogravimetric analysis (TGA) of samples of bulk, mpg- and ompg-CN under a N_2 atmosphere (see Fig. 4). All the samples were found to be stable at temperatures up to 550 °C, suggesting a stable construction from heptazine-base units in the materials.[45] The mass loss below 200 °C is in part due to H_2O and other volatile impurities being absorbed on the sample surface. Further heating of the remaining material results in a complete weight loss finalized at 720 °C, which, however, proves the complete removal of the template SiO_2.

The carbon and nitrogen stoichiometry of prepared mesoporous samples determined by elemental analysis (†see Table S1) shows that all products have an about perfect nitrogen content

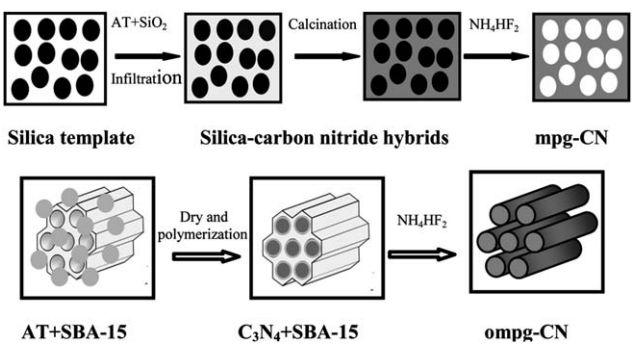

Scheme 2 Schematic diagrams for the fabrication of mpg-CN and ompg-CN from NH_4SCN using nano-sized SiO_2 particles and SBA-15, respectively.

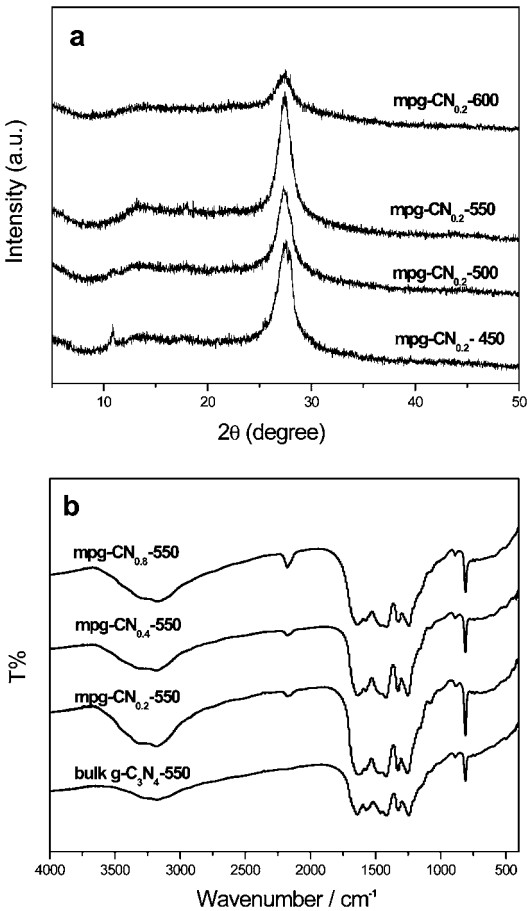

Fig. 3 (a) XRD and (b) FTIR of mpg-CN samples.

(~60% in weight), very close to the ideal C_3N_4 composition. The C/N ratios are around 0.75, the theoretical C/N ratio of the perfect structure of bulk C_3N_4 material. Though trace amounts of elemental S show up in the composition report, the molar ratio of S/C approaches 0.1%, this is within the experimental errors of the machine.

The local morphologies of synthesized materials were investigated by SEM and TEM as shown in Fig. 5. Fig. 5a demonstrates that the bulk g-C_3N_4 was composed of large particles with a layer

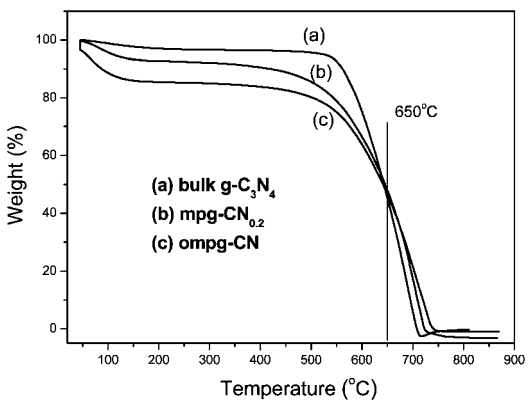

Fig. 4 Thermogravimetric analysis (TGA) results for carbon nitride under nitrogen atmosphere at a heating rate of 10 K min^{-1}.

structure. But after treatment with the silica template, particles of higher uniform dispersion and a smaller size, and a porous mpg-CN surface were observed (Fig. 5b). The regular rod-like objects with ordered pore structure of ompg-CN are shown in Fig. 5c, which corresponds well to the original texture of the SBA-15 template (†Fig. S1). TEM images directly reflect the inner structures of the carbon nitride samples. The presence of a disordered but well-developed pore system of spherical mesopores within mpg-CN is shown in Fig. 5e, and a pore diameter close to 12 nm directly reflects the size of the silica template. The TEM images taken along the (100) direction of ompg-CN confirm the presence of hexagonally arranged ordered pores (Fig. 5f).

The texture and structure of the mpg- and ompg-CN samples were characterized by nitrogen adsorption-desorption measurements. The isotherms and the Barrett-Joyner-Halenda (BJH) pore size distributions are shown in Fig. 6. The isotherms of our mpg- and ompg-CN show typical hysteresis, proving the existence of larger mesopores connected *via* micropores. The Brunauer-Emmett-Teller (BET) surface area, BJH pore sizes, and pore volumes are summarized in Table 1. The average pore diameter and pore volume of mpg-CN samples grow with the more initial silica added and reached the highest value in mpg-$CN_{0.4}$ sample, then decreased. The relation of the BET)surface area (as determined from the desorption branch of the nitrogen

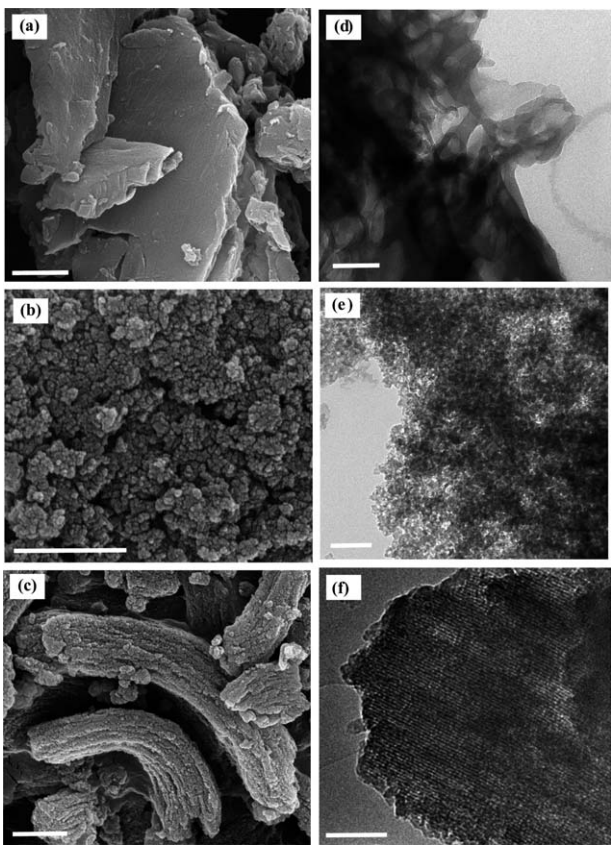

Fig. 5 SEM images of bulk g-C_3N_4 (a), mpg-$CN_{0.2}$ (b), ompg-CN (c) and TEM images of bulk g-C_3N_4 (d), mpg-$CN_{0.2}$ (e), ompg-CN (f). The scale bars of the SEM and TEM images are 500 nm and 100 nm, respectively.

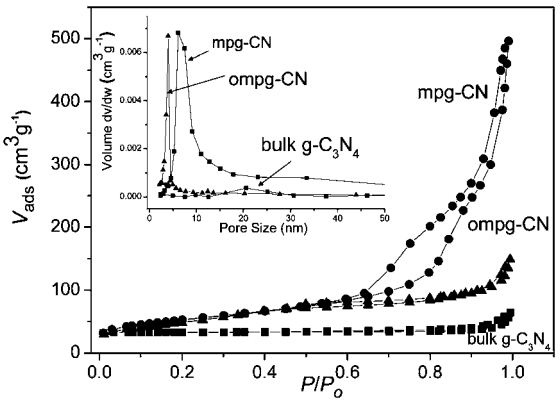

Fig. 6 N_2 adsorption-desorption isotherms for carbon nitride polymers and the corresponding BJH pore-size distribution curves (inset).

adsorption/desorption isothermal) with the content of the template is, however, not at all linear. First, it strongly increases with *r*, and then it decreases again, presumably owing to structural pore collapse (Table 1). The pore walls of carbon nitride turn too thin when excessive silica is introduced and are very susceptible to collapse during SiO_2-removal and the washing processes.

Fig. 7 shows the UV-Vis diffusion spectra of the prepared mesoporous samples. Compared with the bulk g-C_3N_4 particles, the optical band edges and thereby the semiconductor properties of mesoporous materials are maintained but indeed slightly shifted to a shorter wavelength, corresponding to an increase in band gap from 2.62 eV of bulk g-C_3N_4 to 2.75 eV of mpg-CN and 2.78 eV of ompg-CN. The blue shifts can be explained by a decrease of conjugation length or a strong quantum confinement effect in the samples synthesized in the presence of hard templates. Indeed, a similar blue-shift was observed for all the mpg-CN samples with different silica/AT mass ratio (inset, Fig.7). As a result of the lower nm-size, the band gaps of mesoporous carbon nitride are enlarged, and accordingly its redox ability is strengthened. The enlarged band gap, together with the enlarged surface area are favorable for light-harvesting, charge transfer and mass-transport and should in principle alter the photocatalytic performance of carbon nitride polymers significantly.

The operation of semiconductor photocatalysts is due to the creation of photogenerated electron-hole pairs, which transfer from the bulk to the surface of the catalyst and induce surface redox reactions on the surface. It is clear that the photocatalytic activities of semiconductors are greatly influenced by the mobility and number of light-stimulated free carriers. Fig. 8 depicts the photocurrent response of the obtained C_3N_4 sample layers casted on indium tin oxide (FTO) glass plates in a 0.2 M Na_2SO_4 aqueous solution under visible light illumination ($\lambda >$ 420 nm). It clearly shows that the photocurrent generated from porous C_3N_4 samples is much higher than that from bulk materials.

The photocatalytic activity of mpg-$CN_{0.2}$ and ompg-CN compared with bulk g-C_3N_4 (AT) and bulk g-C_3N_4 (DCDA) samples were examined by analyzing the visible-light-induced ($\lambda >$ 420) hydrogen evolution from water/triethanolamine mixture with Pt (3% wt) as a surface electron acceptor and catalytic site for hydrogen evolution (see Fig. 9). Indeed, the

Table 1 Physicochemical properties and photocatalytic activity of bulk and mesoporous graphitic carbon nitride samples for hydrogen evolution with visible light

Catalysts	C/N (atomic)	SA[a](m^2 g^{-1})	PV[b](cm^3 g^{-1})	PD[c](nm)	HER[d](μmol h^{-1})
bulk g-$C_3N_{4(DCDA)}$	0.74	8	–	–	26
bulk g-$C_3N_{4(AT)}$	0.76	9	–	–	58
mpg-$CN_{0.1}$	0.76	152	0.56	12.3	221
mpg-$CN_{0.2}$	0.75	188	0.77	13.8	213
mpg-$CN_{0.4}$	0.75	186	0.82	14.3	207
mpg-$CN_{0.6}$	0.77	133	0.48	11.6	215
mpg-$CN_{0.8}$	0.74	129	0.49	11.9	201
ompg-CN	0.75	171	0.24	5.3	220
mpg-$CN_{(CY)}$	–	204	0.79	13.1	183
ompg-$CN_{(CY)}$	–	239	0.34	5.3	152

[a] BET: surface. [b] Pore volume. [c] Average pore size determined by BJH method. [d] H_2 evolution rate.

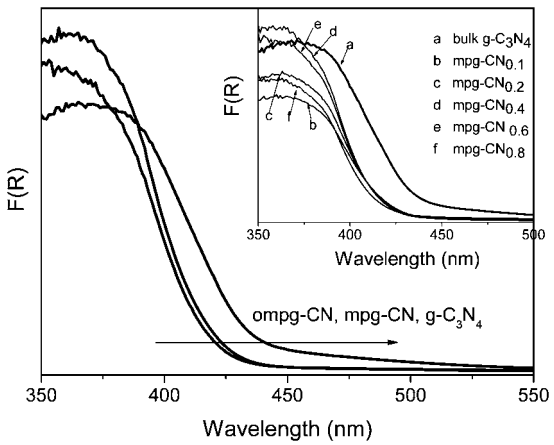

Fig. 7 UV-vis diffuse reflectance spectroscopy for bulk g-C_3N_4, mpg-CN and ompg-CN. The inset is the comparison of optical absorption of bulk g-C_3N_4 with those of mpg-CN samples with different silica/AT mass ratio.

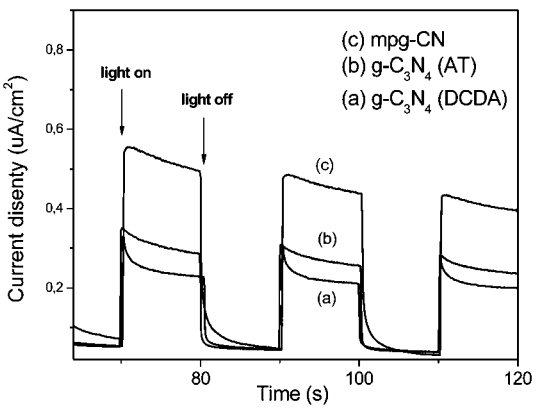

Fig. 8 Transient current response of FTO/C_3N_4 at 0.2 V *vs.* Ag/AgCl (3 M KCl) in 0.2 M $NaSO_4$ under visible light ($\lambda > 420$ nm, 500 W Xe lamp).

g-C_3N_4 (AT) sample shows an improvement in H_2 evolution activity over the reference g-C_3N_4 (DCDA), again reflecting the advantage of using ammonium thiocyanate as the precursor for carbon nitride synthesis. This is certainly consistent with our previous study that carbon nitride photocatalysts synthesized from a sulfur-mediated route presented an enhanced photocatalytic activity for hydrogen evolution. Not unexpectedly, the mpg-CN sample shows again a remarkable improvement of photocatalytic activity over bulk ones. The rate for H_2 evolution of mpg-$CN_{0.2}$ reaches 213 μmol h^{-1}, nearly 3.6 times the rate of bulk material. Though the specific surface area of ompg-CN (171 m^2 g^{-1}) was less than that of mpg-$CN_{0.2}$, ompg-CN even produced 529 μmol H_2 during 5h reaction, slightly higher than mpg-$CN_{0.2}$. This slight enhancement may be attributed to the ordered 1D porous structure that is favorable for supporting fast electron- and mass-transfer in the nanoscale, which plays an important role in the photocatalytic process. The H_2 evolution activity of the series of mesoporous materials obtained through different initial silica template amounts are also shown in Table 1. To our surprise, the differences between the different materials are not significant and did not show any systematic variation. The activities of mpg-CN and ompg-CN synthesized from cyanamide (CY) are also listed in Table 1, they are lower than those of their porous counterparts synthesized from AT, again reflecting the advantage of using AT as the precursor.

With the mpg-$CN_{0.2}$ sample is a catalyst, a 20 h recycling experiment with intermittent evacuation every 5 h was performed under visible light ($\lambda > 420$ nm) to examine the stability of the polymeric catalyst. A total of 1.6 mmol hydrogen gas was produced during the course of the 20 h irradiation, without noticeable catalyst deactivation. The produced H_2 exceeds the amount of carbon nitrides used (0.27 mmol in terms of heptazine

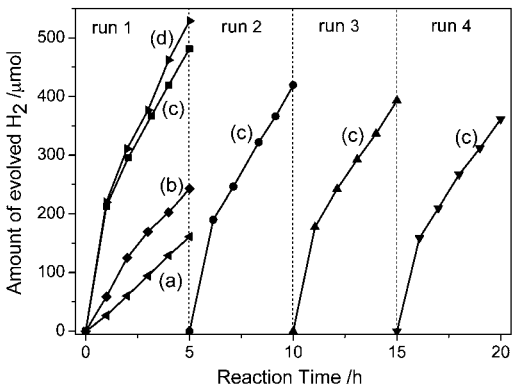

Fig. 9 Amount of evolved H_2 gas using mpg-$CN_{0.2}$ photocatalyst (c) as a function of time, with reference to bulk g-C_3N_4 (DCDA) (a), g-C_3N_4 (AT) (b), ompg-CN (d) in the first run reaction. The consecutive three runs are the stability test for the mpg-$CN_{0.2}$ photocatalyst.

as repeated units), while the turnover frequency (TOF) of H_2 generation was calculated to be 10.4 h^{-1} with respect to Pt atoms added. The photocatalytic H_2 evolution activity of other mpg-$CN_{0.2}$ synthesized at different temperatures was also investigated and is displayed in †Table S2. We can see that treatment at a higher temperature is beneficial for the photocatalytic activity of the mpg-CN catalyst, but too high temperatures degrade carbon nitride semiconductors.

4. Conclusions

A new synthesis of polymeric g-C_3N_4 nanocomposites using direct thermal condensation of ammonium thiocyanate (NH_4SCN) was presented. As NH_4SCN is a cheap salt with a low melting point and high water solubility, this change allows a variety of new aqueous based processes. It was shown that carbon nitrides with about optimal composition and structure were formed *via* the release of H_2S and NH_3 gas. In order to modify the texture of the as-obtained carbon nitrides, the polymerization of NH_4SCN was combined with hard-templating using nanostructural silica as templates to fabricate mesorporous and ordered mesoporous carbon nitrides. High specific surface area and well-developed pore structure could be obtained. Several characterization methods were carried out to examine the obtained porous carbon nitride photocatalyst. The results indicated that the as-prepared porous catalysts had favourable semiconductor properties, although the absorption edges show a little blue-shift. Compared to bulk g-C_3N_4, porous C_3N_4 shows improved photocatalytic activities while keeping high stability at the same time. Considering the ease of solution-processibility and the low price of NH_4SCN, together with the special coordination chemistry of SCN^- ions with transition metals, the development of a wide range of new carbon nitride based hybrid nanomaterials by this route can be envisaged as advanced functional materials for diverse applications ranging from catalysis, photocatalysis, chemical sensing, photovoltaic solar cells up to organic photosynthesis.

Acknowledgements

This work is financially supported by the National Natural Science Foundation of China (21033003 and U1033603), 973 Program (2007CB613306), the Natural Science Foundation of Fujian Province (Grant No. 2010J05030) and the Science & Technology Program of the Education Department of Fujian Province (Grant No.JK 2009031).

References

1 R. M. Navarro, M. A. Peña and J. L. G. Fierro, *Chem. Rev.*, 2007, **107**, 3952.
2 S. Miller, *Environ. Sci. Technol.*, 1983, **17**, 75.
3 A. W. Hains, Z. Q. Liang, M. A. Woodhouse and B. A. Gregg, *Chem. Rev.*, 2010, **110**, 6689.
4 A. I. Hochbaum and P. D. Yang, *Chem. Rev.*, 2010, **110**, 527.
5 A. Fujiashima and K. Honda, *Nature*, 1972, **238**, 37.
6 K. Maeda, K. Teramura, D. L. Lu, T. Takata, N. Saito, Y. Inoue and K. Domen, *Nature*, 2006, **440**, 295.
7 X. B. Chen, S. H. Shen, L. J. Guo and S. S. Mao, *Chem. Rev.*, 2010, **110**, 6503.
8 A. Kudo and Y. Miseki, *Chem. Soc. Rev.*, 2009, **38**, 253.
9 A. J. Esswein and D. G. Nocera, *Chem. Rev.*, 2007, **107**, 4022.
10 H. J. Yan, J. H. Yang, G. J. Ma, G. P. Wu, X. Zong, Z. B. Lei, J. Y. Shi and C. Li, *J. Catal.*, 2009, **266**, 165.
11 S. C. Roy, O. K. Varghese, M. Paulose and C. A. Grimes, *ACS Nano*, 2010, **4**, 1259.
12 N. Ahmed, Y. Shibata, T. Taniguchi and Y. Izumi, *J. Catal.*, 2011, **279**, 123.
13 Q. Liu, Y. Zhou, J. H. Kou, X. Y. Chen, Z. P. Tian, J. Gao, S. C. Yan and Z. G. Zou, *J. Am. Chem. Soc.*, 2010, **132**, 14385.
14 M. Anpo, H. Yamashitaa, K. Ikeuea, Y. Fujii, S. G. Zhang, Y. Ichihashi, D. R. Parka, Y. Suzuki, K. Koyanoc and T. Tatsumi, *Catal. Today*, 1998, **44**, 327.
15 K. Maeda, M. Higashi, D. Lu, R. Abe and K. Domen, *J. Am. Chem. Soc.*, 2010, **132**, 5858.
16 H. Kato, K. Asakura and A. Kudo, *J. Am. Chem. Soc.*, 2003, **125**, 3082.
17 Z. Yi, J. Ye, N. Kikugawa, T. Kako, S. Ouyang, H. Stuart-Williams, H. Yang, J. Cao, W. Luo, Z. Li, Y. Liu and R. Withers, *Nat. Mater.*, 2010, **9**, 559.
18 F. E. Osterloh, *Chem. Mater.*, 2008, **20**, 35.
19 K. Maeda and K. Domen, *Chem. Mater.*, 2010, **22**, 612.
20 J. H. Huang, Y. J. Cui and X. C. Wang, *Environ. Sci. Technol.*, 2010, **44**, 3500.
21 Z. X. Chen, D. Z. Li, W. J. Zhang, C. Chen, W. J. Li, M. Sun, Y. H. He and X. Z. Fu, *Inorg. Chem.*, 2008, **47**, 9766.
22 M. Yoshida, T. Hirai, K. Maeda, N. Saito, J. Kubota, H. Kobayashi, Y. Inoue and K. Domen, *J. Phys. Chem. C*, 2010, **114**, 15510.
23 X. C. Wang, K. Maeda, A. Thomas, K. Takanabe, G. Xin, J. M. Carlsson, K. Domen and M. Antonietti, *Nat. Mater.*, 2008, **8**, 76.
24 K. Xiao, Y. Q. Liu, P. A. Hu, G. Yu, Y. M. Sun and D. B. Zhu, *J. Am. Chem. Soc.*, 2005, **127**, 8614.
25 R. B. Sharma, D. J. Late, D. S. Joag, A. Govindaraj and C. N. R. Rao, *Chem. Phys. Lett.*, 2006, **428**, 102.
26 K. P. Gong, F. Du, Z. H. Xia, M. Durstock and L. M. Dai, *Science*, 2009, **323**, 760.
27 P. H. Matter, E. Wang and U. S. Ozkan, *J. Catal.*, 2006, **243**, 395.
28 K. Maeda, X. C. Wang, Y. Nishihara, D. L. Lu, M. Antonietti and K. Domen, *J. Phys. Chem. C*, 2009, **113**, 4940.
29 J. S. Zhang, J. H. Sun, K. Maeda, K. Domen, P. Liu, M. Antonietti, X. Z. Fu and X. C. Wang, *Energy Environ. Sci.*, 2011, **4**, 675.
30 A. Vinu, *Adv. Funct. Mater.*, 2008, **18**, 816.
31 A. Vinu, K. Ariga, T. Mori, D. Golberg, Y. Bando, T. Nakanishi and S. Hishita, *Adv. Mater.*, 2005, **17**, 1648.
32 A. Vinu, P. Srinivasu, D. P. Sawant, T. Mori, K. Ariga, J. S. Chang, S. H. Jhung, Y. K. Hwang and V. V. Balasubramanian, *Chem. Mater.*, 2007, **19**, 4367.
33 S. Hwang, J. S. Lee and J. S. Yu, *Appl. Surf. Sci.*, 2007, **253**, 5656.
34 F. Goettmanm, A. Fischer, M. Antonietti and A. Thomas, *Angew. Chem., Int. Ed.*, 2006, **45**, 4467.
35 M. Groenewolt and M. Antonietti, *Adv. Mater.*, 2005, **17**, 1789.
36 X. F. Chen, Y. S. Jun, K. Takanabe, K. Maeda, K. Domen, X. Z. Fu, M. Antonietti and X. C. Wang, *Chem. Mater.*, 2009, **21**, 4093.
37 E. Z. Lee, Y. S. Jun, W. H. Hong, A. Thomas and M. M. Jin, *Angew. Chem. Int. Ed.*, 2011, **50**, 9706.
38 Z. Zhang, K. Leinenweber, M. Bauer, L. A. J. Garvie, P. F. McMillan and G. H. Wolf, *J. Am. Chem. Soc.*, 2001, **123**, 7788.
39 J. L. Zimmerman, R. Williams, V. N. Khabashesku and J. L. Margrave, *Nano Lett.*, 2001, **1**, 731.
40 J. Liebig, *A. Pharm and Lemgo Ger.*, 1834, **10**, 1.
41 E. C. Franklin, *J. Am. Chem. Soc.*, 1922, **44**, 486.
42 A. A. Grizik and G. P. Borodulenko, *Tsvetnye Metally*, 1972, **45**, 41.
43 A. Galarneau, H. Cambon, F. D. Renzo, R. Ryoo, M. Choi and F. Fajula, *New J. Chem.*, 2003, **27**, 73.
44 F. Goettmann, A. Fischer, M. Antonietti and A. Thomas, *Chem. Commun.*, 2006, 4530.
45 J. R. Holst and E. G. Gillan, *J. Am. Chem. Soc.*, 2008, **130**, 7373.
46 M. J. Bojdys, J. Muller, M. Antonietti and A. Thomas, *Chem.–Eur. J.*, 2008, **14**, 8177.
47 S. W. Bian, Z. Ma and W. G. Song, *J. Phys. Chem. C*, 2009, **113**, 8668.
48 D. R. Miller, J. J. Wang and E. G. Gillan, *J. Mater. Chem.*, 2002, **12**, 2463.
49 S. M. Lyth, Y. Nabae, S. Moriya, S. Kuroki, M. Kakimoto, J. Ozaki and S. Miyata, *J. Phys. Chem. C*, 2009, **113**, 20148.
50 D. Foy, *J. Solid State Chem.*, 2009, **182**, 165.
51 M. J. Bojdys, J. Q. Müller, M. Antonietti and A. Thomas, *Chem.–Eur. J.*, 2008, **14**, 8177.